MRS Advances © 2018 Materials Research Society
DOI: 10.1557/adv.2018.513

Investigation of Perovskite Solar Cells Employing Chemical Vapor Deposited Methylammonium Bismuth Iodide Layers

Dominik Stümmler[1], Simon Sanders[1], Pascal Pfeiffer[1], Noah Wickel[1], Gintautas Simkus[1,2], Michael Heuken[1,2], Peter K. Baumann[3], Andrei Vescan[1], Holger Kalisch[1]

[1]*Compound Semiconductor Technology, RWTH Aachen University, Sommerfeldstr. 18, 52074 Aachen, Germany.*

[2]*AIXTRON SE, Dornkaulstr. 2, 52134 Herzogenrath, Germany.*

[3]*APEVA SE, Dornkaulstr. 2, 52134 Herzogenrath, Germany.*

ABSTRACT

Although Pb-based perovskite solar cells already achieve power conversion efficiencies (PCE) beyond 20 %, the use of toxic Pb is causing considerable environmental concern. As a consequence, a variety of alternative cations have been investigated to replace Pb^{2+} in the perovskite structure. Methylammonium bismuth iodide ($MA_3Bi_2I_9$, MBI) has shown promising results for environmentally benign and chemically stable devices. While the PCE of MBI-based solar cells are still comparably low, structural improvements have been made by using chemical vapor deposition (CVD). CVD allows for the well-controlled formation of coherent and dense MBI layers in contrast to solution-processing. In this work, CVD as a possible MBI fabrication method for efficient and size-scalable solar cells is discussed. The precursors MA iodide (MAI) and Bi iodide (BiI_3) are deposited in an alternating deposition process forming the desired MBI perovskite on the heated substrate. Substrate temperatures as well as deposition times of each precursor are varied with the aim of forming coherent and dense MBI layers. Optimized films are further processed to solar cell prototypes and compared with solution-processed reference devices. The results reveal that CVD possesses great potential to enable the manufacture of MBI photovoltaic (PV) devices processed in a solvent-free environment.

INTRODUCTION

Perovskite solar cells have become a prominent subject in photovoltaic (PV) research because of a rapid development of PCE figures. Benchmark devices reach PCE significantly >20 % [1]. For the widely used organo lead halide perovskites, solution-

based (e.g. spin-coating) as well as vapor phase deposition have been demonstrated [2]. Recently, less toxic replacements for Pb and solvent-free processes have come into focus to overcome toxicity issues [3]. In this context, replacing Pb with less toxic Bi showed superior stability [4]. While lifetime improved strongly, PCE figures are still rather low, rarely exceeding the value of 1 % [5]. Solution-processing of MBI leads to films with poor substrate coverage, small crystal grains, deteriorated electronic properties and PV performance [6]. Efforts to optimize MBI solar cells are therefore mainly focused on their structural properties and film morphology. Deposition from the vapor phase has been demonstrated to form high-density layers with enhanced coverage [7]. These MBI-based solar cells also demonstrated superior PCE (up to 1.64 %) compared to solution-processed ones, thus proving the great potential of gas phase deposition techniques for MBI. In this work, we analyse the influence of substrate temperature and deposition times on CVD MBI in a setup which has already been successfully used for the deposition of MAPI (methylammonium lead iodide) [8]. As a reference, solution-processed MBI layers are also fabricated. Solution-processed and CVD MBI layers are finally compared regarding their PV performance.

EXPERIMENTAL DETAILS

A custom-built CVD tool for perovskites is employed to deposit MBI, tailored to the different vapor pressure regimes [9, 10] of both precursors. Nitrogen is used as carrier gas, and the process chamber pressure is set to 10 hPa. BiI_3 is placed in a crucible which allows for evaporation into a hot carrier gas stream, and the source is heated to 250 °C. MAI is loaded into a powder evaporation source, held at 150 °C also in nitrogen carrier gas. During deposition, the source nitrogen flows are set to 500 sccm in each source. The substrate temperature can be controlled in the range of 10 to 80 °C. Due to the low Reynolds number of the process, a laminar flow regime is expected inside the deposition chamber, most likely resulting in only negligible intermixing of the individual mass flows on their way to the substrate [11]. Therefore, the two precursors are deposited in an alternating deposition scheme in which both species are deposited consecutively over defined periods (deposition cycles) with time lengths between 300 s and 9,000 s. The total deposition time has been set to 5 h. In this study, both constituents are deposited with identical durations (e. g. a deposition cycle of 300 s of BiI_3 followed by a 300 s cycle of MAI). While depositions of the single components BiI_3 and MAI are carried out on bare FTO substrates, perovskite formation is optimized on TiO_2-coated FTO. Pre-cut FTO substrates (2.5 cm x 2.5 cm) are cleaned in DMSO (170 °C), acetone (80 °C) and iso-propanol (80 °C) baths and rinsed with de-ionized water for 10 min. each. For TiO_2 coating, a 15 nm Ti layer is thermally evaporated under high vacuum ($p < 10^{-6}$ hPa). On top of this compact Ti layer, diluted titania paste (Sigma-Aldrich, 1 g paste in 5 ml 2-methoxyethanol) is spin-coated at 2000 rpm in N_2 atmosphere. The deposited layers are annealed at 130 °C for 5 min. and at 500 °C for 30 min in air. For the solution-processed MBI films, 235.9 mg BiI_3 and 95.4 mg MAI are dissolved in 1 mL dimethylformamide (DMF) in nitrogen. Prior to spin-coating at 5000 rpm for 30 s, the solution is heated to 100 °C. The solution-processed MBI layers are then annealed at 100 °C for 10 min. in a N_2-filled glovebox. It should be mentioned that CVD MBI layers are transported to the N_2 atmosphere after MBI deposition with short exposition to air. Due to the superior air stability of MBI, only limited impact of this exposure is expected. For both types of MBI samples, as p-type doped HTM (hole transport material), 83.3 mg Spiro-MeOTAD, 11.13 mg TBP (tert-butylpyridine) and 7.5 mg Li-TFSI (lithium-bis-trifluoromethanesulfonyl-imide) are dissolved in 1 mL of a mixture of chlorobenzene and

acetonitrile (10:1 volume ratio) [12]. The solution is spin-coated on the perovskite at 2000 rpm for 30 s and dried afterwards at room temperature for 30 min. For cathode deposition, 60 nm Au are evaporated via e-beam ($p < 10^{-6}$ hPa). Active areas (0.19 cm^2) are defined via a shadow mask during the cathode deposition. The morphology of the perovskite layers is characterized by scanning electron microscopy (SEM). IV curves of the solar cells are measured with a Keithley 2400 Sourcemeter under AM1.5 illumination. Thicknesses are determined via SEM cross-section images.

DISCUSSION

Single Depositions of BiI_3 and MAI

Prior to depositing MBI, single deposition experiments of MAI and BiI_3 are conducted to calibrate the deposition rates of the individual precursors. MAI deposition on FTO at a substrate temperature of 15 °C leads to homogeneous layers. Deposition rates are determined to be approx. 300 nm/h. For the single deposition of BiI_3 on FTO, the resulting deposition rate at a substrate temperature of 15 °C is about 60 nm/h, which can be attributed to its significantly lower vapor pressure (identical flows of 500 sccm).

Variation of substrate temperature

MBI layers are deposited for 5 h at substrate temperatures of 15, 30, 50 and 80 °C with deposition cycles of 3600 s (Fig. 1). The cyclic deposition process is starting with BiI_3. MBI deposition rates are determined to be in the range of 40 nm/h, which is much lower than the average of the precursor deposition rates measured before.

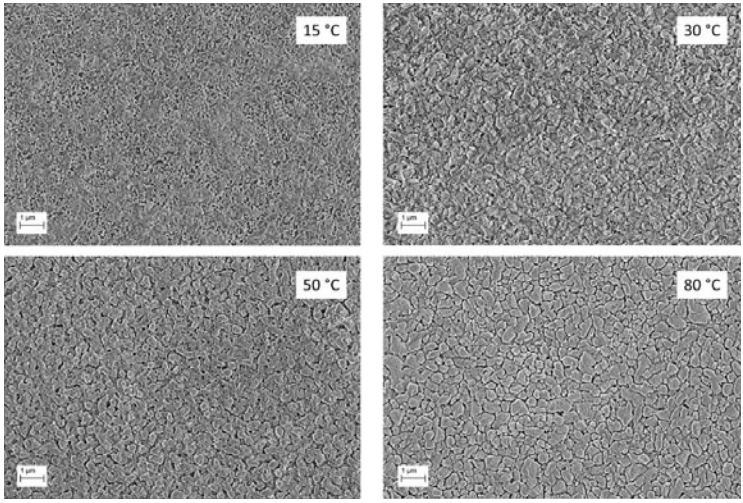

Figure 1: SEM pictures of MBI films deposited at different substrate temperatures

The final thickness for all samples was ~200 nm with only small deviations between the samples. We expect MBI formation to be limited by BiI_3, the less volatile constituent with the lower individual growth rate which is converted to MBI by the MAI partial pressure. Normalized to the BiI_3 deposition cycles only, an MBI deposition rate of 80 nm/h (BiI_3: ~60 nm/h) can be extracted. At a low substrate temperature of 15°C, small particles (50-100 nm) can be observed in SEM images (Fig. 1) as well as larger dark spots corresponding to uncovered areas. The MBI structure is porous and the layer is not entirely closed. It might be the case that at low temperatures, excess MAI is neither re-evaporated properly from the surface before the following BiI_3 deposition cycle nor consumed for MBI formation. With increased substrate temperatures at 30 °C and 50 °C, crystal grains are growing more rapidly and the surface coverage is enhanced. While small particles still can be seen in the structure deposited at 30 °C, large crystals are grown at 50 °C. At the highest temperature (80 °C), largest grain size and uniformity of the film can be achieved, with crystals nearly reaching a diameter of 1 µm. In conclusion, higher substrate temperatures (80 °C) promote crystal growth and re-evaporation of MAI, which is beneficial for MBI stoichiometry.

Variation of deposition cycles

Different deposition cycles (Fig. 2) are chosen, using the optimized substrate temperature of 80 °C. The total deposition time has been set to 5 h for each sample and the layer thicknesses of the samples have been measured to be in the range of 200 nm.

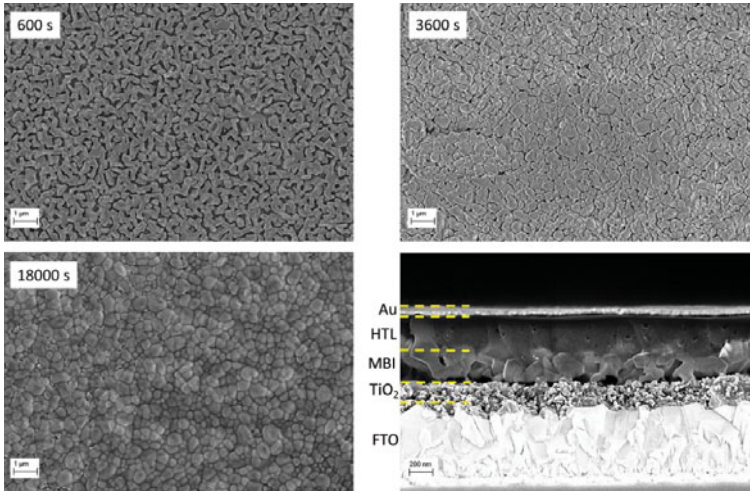

Figure 2: SEM pictures of MBI films at different deposition cycles. Bottom-right: Cross-section image of a complete solar cell showing the gaps of MBI at the titanium dioxide interface.

As it can be clearly seen in the SEM images, coverage of MBI layers increases with longer deposition cycles whereas at shorter cycles, MBI nuclei tend to grow primarily in vertical direction. From literature, it is known that BiI_3 preferably grows in vertical direction at higher temperatures [13]. As a consequence, during BiI_3 deposition

cycles crystals are formed perpendicular to the surface. With longer deposition cycles of MAI, MBI crystals also grow in horizontal direction and close the gaps between the crystal grains. Cross-sectional images reveal that closed and conformal layers are not entirely achieved throughout the film thickness. Especially, at the interface to the TiO_2 layer relatively large gaps remain (Fig. 2), consistent with the proposed preferentially vertical growth mechanism. Assuming a 3D-growth of the MBI nuclei, coalescence of the grains is only achieved above a certain time of MAI deposition and the crystals remain incoherent near the titania interface. These gaps between the MBI crystals result in a poor electrical contact between the mesoporous TiO_2 structure and the active layer, which leads to cells with low current densities. This is discussed in the following section.

Fabrication of solar cells and comparison with solution processing

To evaluate the solar cell performance of the CVD MBI layers, solar cells using solution-processed MBI are also fabricated. Solution processing of MBI leads to structures with significantly different morphology. The structure is composed of flat needle-shaped crystal grains which are oriented in parallel to the surface with limited contact between each other. Nonetheless, these solar cell show reliable performance with short-circuit currents comparable to those of devices reported in literature, but fill factors remain low. This might be attributed to the large gaps in the active layer, facilitating short-circuits between the HTM and the mesoporous TiO_2 matrix. On the other hand, devices with CVD MBI exhibit rather low currents and generally higher fill factors. While the higher fill factors can be explained by the coalesced films preventing shunts between the HTM and TiO_2, diverse structural defects may cause the low currents. First, the active layer is not entirely in contact with the TiO_2, and electron transport between both layers is hampered. Second, it might be assumed that MBI does not penetrate the mesoporous titanium structure properly as it can be observed in solution-processed solar cells. Thus, the diffusion pathways of excitons are increased. Since the exciton binding energy is much higher in MBI, this has a more pronounced effect on the extracted current than it would have e. g. on MAPI devices [14]. For the CVD MBI, the highest open-circuit voltage measured is 0.71 V (identical with solution-process MBI) and is achieved with 80 °C substrate temperature and a deposition cycle of 3600 s. The largest PCE is 0.0471 %. This cell has been fabricated with lower deposition cycles of 1200 s. The best cells with solution-processed MBI have shown a remarkable PCE of 0.169 % which is significantly higher than those of the CVD cells (Fig. 3).

CONCLUSION

The experiments conducted in this work show that CVD is a promising for MBI-based solar cells. However, PCE of the produced cells remain low which can be attributed to poor adhesion and interpenetration between the MBI and the titania electrode. Future work should include further optimization of the reaction engineering aiming at better coverage of MBI on the mesoporous TiO_2 and a complete process without air exposure. In conclusion, cells fabricated with CVD MBI showed promising results such as relatively high open-circuit voltages and improved fill factors.

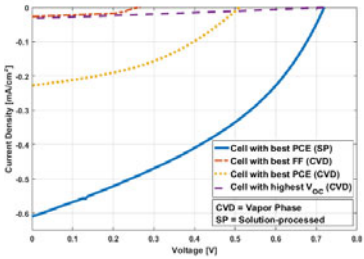

	CVD			SP
	Best PCE	Best FF	Best V_{oc}	Best PCE
PCE[%]	4.71×10^{-2}	3.40×10^{-3}	5.95×10^{-3}	0.17
FF[%]	40.54	48.95	26.49	38.57
V_{OC} [V]	0.51	0.27	0.71	0.72
I_{sc} [mA/cm²]	0.23	2.60×10^{-2}	3.13×10^{-2}	0.61
Dep. Cycle[s]	1200	3600	3600	-
Sub.-Temp [°C]	80	80	80	-

Figure 3: IV-Curves of solar cells with best FF, PCE and V_{OC} fabricated by solution-processing and CVD

ACKNOWLEDGMENTS

The authors acknowledge the financial support of the European Union through the European Regional Development Fund (ERDF) "Investing in our Future" in the EFRE.NRW 2014-2020 program for the project PeroBOOST (EFRE-0800127, EFRE-0801060).

REFERENCES

1. M. A. Green, Y. Hishikawa, E. D. Dunlop, D. H. Levi, J. Hohl-Ebinger, and A. W.Y. Ho-Baillie, *Prog. Photovolt. Res. Appl.* **26** (1), 3–12 (2018).
2. J. Ávila, C. Momblona, P. P. Boix, M. Sessolo, and H. J. Bolink, *Joule* **1** (3), 431–442 (2017).
3. F. Giustino and H. J. Snaith, *ACS Energy Lett.* **1** (6), 1233–1240 (2016).
4. R. L. Z. Hoye, R. E. Brandt, A. Osherov, V. Stevanović, S. D. Stranks, M. W. B. Wilson, H. Kim, A. J. Akey, J. D. Perkins, R. C. Kurchin, J. R. Poindexter, E. N. Wang, M. G. Bawendi, V. Bulović, and T. Buonassisi, *Chemistry* **22** (8), 2605–2610 (2016).
5. H. Hu, B. Dong, and W. Zhang, *J. Mater. Chem. A* **5** (23), 11436–11449 (2017).
6. M. Pazoki, M. B. Johansson, H. Zhu, P. Broqvist, T. Edvinsson, G. Boschloo, and E. M. J. Johansson, *J. Phys. Chem. C* **120** (51), 29039–29046 (2016).
7. Z. Zhang, X. Li, X. Xia, Z. Wang, Z. Huang, B. Lei, and Y. Gao, *J. Phys. Chem. Lett.* **8** (17), 4300–4307 (2017).
8. D. Stümmler, S. Sanders, P. Pfeiffer, M. Weingarten, A. Vescan, and H. Kalisch, *MRS Adv.* **2** (21-22), 1189–1194 (2017).
9. A. Dualeh, P. Gao, S. I. Seok, M. K. Nazeeruddin, and M. Grätzel, *Chem. Mater.* **26** (21), 6160–6164 (2014).
10. J. H. Kim and S. Blairs, *J. Chem. Thermodyn.* **22** (8), 803–814 (1990).
11. H. O. Pierson, *Handbook of chemical vapor deposition (CVD). Principles, technology, and applications*, 2. ed. (Noyes Publ, Norwich, NY, 1999).
12. J.-H. Im, H.-S. Kim, and N.-G. Park, *APL Mater.* **2** (8), 81510 (2014).
13. A. Cuña, I. Aguiar, A. Gancharov, M. Pérez, and L. Fornaro, *Cryst. Res. Technol.* **39** (10), 899–905 (2004).
14. M. Lyu, J.-H. Yun, M. Cai, Y. Jiao, P. V. Bernhardt, M. Zhang, Q. Wang, A. Du, H. Wang, G. Liu, and L. Wang, *Nano Res.* **9** (3), 692–702 (2016).